Colloids and Surfaces A: Physicochemical and Engineering Aspects 737 (2026) 139730

Contents lists available at ScienceDirect

Colloids and Surfaces A: Physicochemical and Engineering Aspects

journal homepage: www.elsevier.com/locate/colsurfa

Escin solutions: Effects of pH and electrolytes on their behavior

Fatmegyul Mustan [a,b], Petar Borisov [a,b], Zlatina Mitrinova [a,c], Slavka Tcholakova [a,*]

[a] Department of Chemical and Pharmaceutical Engineering Faculty of Chemistry and Pharmacy, Sofia University, 1 James Bourchier Ave., Sofia 1164, Bulgaria
[b] Centre of Competence "Sustainable Utilization of Bio-resources and Waste of Medicinal and Aromatic Plants for Innovative Bioactive Products" (BIORESOURCES BG), Sofia, Bulgaria
[c] National Centre of Excellence Mechatronics and Clean Technologies, Sofia University, Bulgaria

GRAPHICAL ABSTRACT

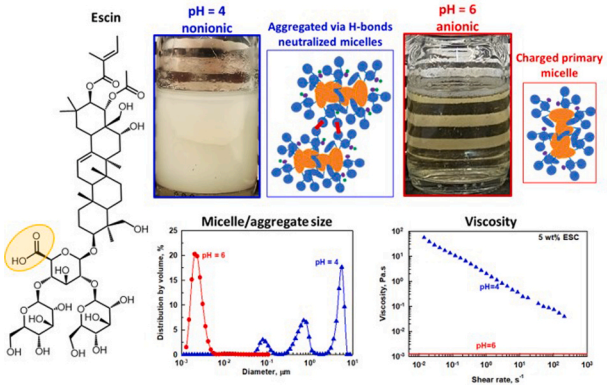

ARTICLE INFO

Keywords:
Saponin
Escin
Solution rheology
Anionic surfactant
Viscous solutions

ABSTRACT

Escin is a triterpenoid saponin with one carboxyl group which is non-ionized at pH < 4.7 and becomes ionized at pH > 4.7. The major aim of the current study is to determine how the electrolyte concentration affects the properties of concentrated escin solutions (5 wt% and 10 wt%) at pHs of 4, 6, and 8. Ionized escin molecules at pH > 4.7 form charged micelles that repel one another when there is no added electrolyte and solutions remain clear and stable for more than a month. Lowering the pH to 4 leads to formation of uncharged micelles. These micelles attract each other and form inter-micellar hydrogen bonds, which enable formation of micrometer aggregates that cause turbidity and phase separation. The addition of background electrolytes to the solutions at pHs of 6 and 8 screens the electrostatic repulsion between micelles, causing partial aggregation of the micelles and gelation of solutions. As the salt concentration increases, the viscosity of the escin solution also increases, reaching a maximum—similar to the behavior observed with conventional surfactants. However, the mechanism behind this viscosity maximum is different. In solutions of conventional surfactants, the maximum is due to the formation of worm-like micelles, whereas the maximum for escin solutions is due to formation of a network of escin aggregates that imparts yield stress and elasticity to the solution. These dispersions remain stable for at least one month at room temperature and can be used as cosmetic and detergent formulations.

* Corresponding author.
E-mail address: SC@LCPE.UNI-SOFIA.BG (S. Tcholakova).

https://doi.org/10.1016/j.colsurfa.2026.139730
Received 1 December 2025; Received in revised form 10 January 2026; Accepted 26 January 2026
Available online 27 January 2026

1. Introduction

Escin is an amphiphilic molecule extracted from horse chestnut [1], consisting of a hydrophobic triterpenoid backbone and a hydrophilic sugar moiety that contains one carboxylic group. The pKa of escin is 4.7 ± 0.2 [2] and it is non-ionized at pH < 4.7 and ionized at pH > 4.7. Non-ionized escin molecules form condensed adsorption layers at air-water interface with very high shear [3] and dilatational elasticities [4], and low gas permeability [5]. These dense adsorption layers reduce the rate of Ostwald ripening in foams [5]. Molecular dynamics simulations have shown that these unique properties are due to strong hydrogen bonding between the oligosaccharide residues of the non-ionized escin molecules, along with pronounced hydrophobic interactions between their triterpenoid skeletons [6]. The ionization of escin molecules significantly affects the properties of the adsorption layers at the air–water interface [5]. As the pH increases above the pKa, surface elasticity decreases, gas permeability increases, leading to faster foam destabilization [5]. These substantial changes in interfacial properties are attributed to dominant electrostatic repulsion between the charged escin molecules, which results in the formation of looser, less cohesive adsorption layers [7].

The change of pH affects not only the interfacial properties of escin molecules adsorbed at air-water interface but also the critical micellar concentration, which increases with pH due to the deprotonation of the carboxyl group in escin molecule [8]. The shape and size of escin micelles are influenced by both temperature and escin concentration [2]. It was shown that at pH of 7.4 and 10 °C, escin forms rod-like micelles with radius of gyration, R_g, of approximately 3.1 nm [2]. Rising the temperature to 40 °C results in the formation of ellipsoidal micelles with smaller $R_g \approx 2.1$ nm and aspect ratio of around 2 [2]. Relatively big in size micelles with length of 20 nm were visualized by TEM images in work of De Groot et al. [9] for escin dissolved in water at ambient temperature. The effect of escin concentration (between 5 and 25 mM) on the micellar size and shape was studied at 25 °C in presence and absence of 100 mM NaCl at natural pH [10]. Without added electrolyte, escin consistently forms rod-like micelles with a short-axis radius of 2.5 nm and an aspect ratio of 12, across all studied concentrations [10]. The addition of 100 mM NaCl had no significant effect at 5 and 10 mM escin, but at 25 mM, the aspect ratio increased to 24, suggesting a transition toward larger self-assembled structures, possibly lamellar or liposomal phases [10]. However, this study did not include further experiments to confirm the exact nature of aggregates formed at high escin and high electrolyte concentrations.

It is well known from the literature that the addition of electrolyte significantly changes the properties of the charged synthetic surfactants due to formation of worm-like micelles, which increases significantly the solution viscosity [11,12]. It is not clear whether the escin molecules can formed worm-like micelles when they are in ionized state as synthetic surfactants do. On the other hand, it is known that the triterpenoid saponin, glycyrrhizic acid, which is similar in structure with escin, is able to form gels upon lowering the pH [13] due to formation of rod-like micelles [14]. The recent study of Tucker et al. [15] showed that the addition of gelation agents, such as background electrolytes and citric acid to glycyrrhizic acid solutions, is accompanying with modest micellar growth and their data show no evidence of longer rod-like or fibrillar structure in these solutions [10].

The major aim of the current study is to determine the effects of addition of mono- and di-valent electrolytes at three pHs (4, 6 and 8) – one below its pKa and two above it on the micellar properties and respective rheological properties of escin solutions with concentrations of 5 wt% (45 mM) and 10 wt% (90 mM). To achieve this aim, the following series of experiments were performed: rheological measurements to determine the viscosity and shear moduli of the solutions, optical observations under optical and cryo-transmission electron microscopy to visualize the aggregates and micelles, SAXS to determine the size and shape of the aggregates.

2. Materials and methods

2.1. Materials

The escin, ESC, was obtained from Rumex extracts, Bulgaria, with a purity of 96 %, and was used without further purification. The molecular mass of escin is 1131.26 g/mol and its molecular structure is shown in Figure S1 in the supporting information (SI). For determining the effect of small fraction of polyphenols that present in Rumex extract some of experiments were performed with escin from Sigma-Aldrich (CAS No. 6805–41–0; Lot No. BCBS3452V, purity 95 %) which does not contain polyphenols. Three different salts were used: potassium chloride (product of Fluka), calcium chloride dihydrate (product of Chem-Lab, purity of 100 %) and magnesium dichloride (product of Valerus, purity of 100 %). Citric acid, CA, (product of Valerus, purity of 100 %) and triethanolamine, TEA, (product of POCH, purity of 100 %) were used to adjust the pH of the solutions. The solutions were prepared with deionized water from Elix 3 water purification system (Millipore, USA).

2.2. Procedure for solution preparation

The escin solutions were prepared by the following procedure: 1) A certain amount of ESC was weighted in a glass beaker; 2) Electrolyte solution was added to achieve the desired ionic strength; 3) The sample was homogenized by stirring with magnetic stirrer at room temperature. At this stage the escin is not well dissolved in the aqueous phase and turbid dispersion was formed; 4) Concentrated TEA solution (100 %) was added to turbid dispersion to reach pH 8, where the solution becomes transparent due to ionization of escin molecules; 5) Crystals of CA were added in order to decrease the pH to 4 or 6. The prepared solutions were stored at room temperature for 24 h and used for the set of experiments to characterize their properties.

2.3. Optical observations

Samples from the solutions were transferred onto microscope glass slides and were observed by optical microscope Axio Imager M2m (Zeiss, Germany) in transmitted light by using long-focus objectives $\times 20$, $\times 50$ or $\times 100$ to detect presence of micrometric aggregates.

2.4. Cryo-TEM imaging

Vitrobot system (FEI, USA) was used for specimen preparation at 25 °C and 100 % relative humidity. Briefly, a drop of the tested solution sample was placed on a holey carbon copper TEM grid, the excess liquid was blotted off with filter paper and then the sample was plunged into a liquid propane-ethane mixture to form a vitrified specimen. Afterwards, the specimen was transferred into a liquid nitrogen and stored in it until further inspection. The cryo-TEM imaging was performed using Gatan cryo-specimen holder at JEM2100, JEOL high-resolution transmission electron microscope. An acceleration voltage of 200 kV was used. Micrographs were recorded with Gatan Orius SC1000 camera.

2.5. Dynamic Light Scattering and ζ-potential measurements

The size of the escin micelles was measured by Zetasizer Nano ZS instrument (Malvern, UK). The transparent solutions were measured without any treatment whereas the turbid solution at pH 4 was diluted 10-times to obtain slightly opalescent solution. All experiments were performed at 25 °C with 2 min of thermal equilibration before the measurement. For each sample at least 3 measurements were conducted and average value and standard deviation were calculated.

The zeta-potentials of the studied samples were conducted using a Zetasizer Nano ZS (Malvern Panalytical, UK) by using disposable folded capillary cells (DTS1070). or each sample, at least three independent measurements were performed to ensure accuracy and reproducibility.

All experiments were performed at 20°C temperature. The Smoluchowski equation was used to covert the measured electrophoretic mobility into a zeta potential, ζ.

2.6. Small-angle X-ray scattering (SAXS)

SAXS measurements of escin solutions were carried out on an inhouse X-ray scattering system (XEUSS 3.0 SAXS/WAXS System, Xenocs, Sassenage, France) with a CuKα X-ray source (λ=0.154 nm, Xeuss 3.0 UHR Dual source Mo/Cu, Xenocs, Sassenage, France) and an Eiger2 4 M detector (Dectris Ltd., Baden Deattwil, Switzerland) with slit collimation. The apparatus was operated at 50 kV and 0.6 mA at 1500 mm or 3000 mm sample to detector distance (SDD) allowed to access the q-range of 0.01 – 0.3 $Å^{-1}$. Data acquisition time was set to 30 min. Silver behenate was used as standard to determine the SDD and the coordinates of the beam center on the detector. The scattered intensity was normalized to the incident intensity, and were corrected for the background scattering from the capillary. Samples were enclosed into vacuum tight thin quartz capillary with an outer diameter of 1 mm and thickness of 10 μm. The measurements were performed at temperature 20 °C. For the SAXS data modeling the software SASView was used.

2.7. Rheological measurements

2.7.1. Steady shear experiments

The viscosity of the solutions was measured with a rotational rheometer (Bohlin Geminin, Malvern UK) by cone and plate geometry with 40 mm or 60 mm diameter, 4° cone angle and 150 μm truncation gap, 1° cone angle with 70 μm truncation gap, respectively. The experiments were performed using a cone-and-plate geometry because this configuration ensures a uniform shear rate in the sheared sample. The measurements were conducted at 20 °C and before each measurement, the sample was left to equilibrate for 1 min at this temperature. The following measurement protocol was used: the rheological test in a steady shear regime was performed by varying the shear rate logarithmically and stepwise from 0.01 s^{-1} to 1000 s^{-1}. The delay time for each step was 2 s and the integration time was 3 s. The viscosity was monitored as a function of the shear rate. At least two measurements were performed with each sample and average viscosities taken at 100 s^{-1} shear rates were plotted as a function of the ionic strength. This rate falls within the typical range of shear rates for mixing, stirring, and pumping home-care and cosmetic formulations.

2.7.2. Oscillatory regime experiments

The storage and loss moduli of the viscous solutions were measured as a function of both frequency of the applied deformation and the strain by using the same rheometer and cone and plate geometry with a diameter of 40 mm, cone angle 4°, truncation gap 150 μm. The amplitude sweep experiments were performed at 1 Hz frequency, while frequency sweep at 1 % deformation.

3. Experimental results

3.1. Effect of pH (no background electrolyte)

The effect of pH was studied for solutions without added background electrolyte at escin concentration of 5 wt% (45 mM). The prepared solutions at pHs 6 and 8 are transparent, whereas the turbid solutions are formed at pH 4, which is below the pKa of escin, see Fig. 1 **A**. The brownish color of the solutions observed at pHs 6 and 8 is due to the presence of polyphenols in the used extract.

The clear solutions of ionized escin molecules at pHs 6 and 8 behaved as water-like fluids. Their viscosities were measured by capillary viscometer to be of 1.26 ± 0.02 mPa•s at pH 6 and 1.30 ± 0.02 mPa•s at pH 8. The turbid solution formed at pH 4 is much more viscous and possesses shear thinning behavior. The viscosity decreases from 8 × 10^4 mPa•s at 0.01 s^{-1} down to 73 mPa•s at 100 s^{-1}, Fig. 1**C**.

The decrease of pH down to 4 was performed by addition of citric acid which is known to induce gelation for glycyrrhizic acid solutions [15]. To determine whether the observed increase in the viscosity of escin solution upon pH decrease was caused by citric acid, we performed a control experiment by using HCl to lower the pH. As can be seen from data presented in Figure S2 in the SI, there is almost no difference in the rheological response of solutions prepared with citric or HCl, which shows that the increase in the viscosity is related to the neutralization of escin molecules and not to gelation properties of citric acid.

The optical observations under transmitted light of 5 wt% escin solutions at pH 6 and 8 showed no micrometer aggregates in these solutions, see Figure S3 in the SI. The cryo-TEM images revealed the presence of almost spherical objects with diameter of ≈ 20 nm, see Fig. 2**A**. DLS measurements showed the presence of two well defined peaks in the distribution by intensity at both pHs, see Fig. 2**B**. The second peak is around 20 nm, which is very similar to the size of spherical objects observed by cryo-TEM and the first peak is at 4.2 nm for sample at pH 6 and at 2.8 nm for sample at pH 8. DLS is highly sensitive to large aggregates because the scattering intensity is proportional to the sixth power of the particle diameter. Consequently, even a small fraction of 20 nm particles contributes significantly to the DLS intensity distribution. This minor fraction of 20 nm particles does not contribute to the DLS volume distribution, as can be seen from data presented in Fig. 2. This shows that the main fraction of escin molecules is incorporated into small spherical micelles with a size of 3–4 nm. The distribution by volume is well described by log-normal distribution:

$$f(x) = a\exp\left[-0.5\left(\frac{\ln(x/x_0)}{\sigma}\right)^2\right] \quad (1)$$

Where x_0 is the mode of the micellar size distribution and σ is the normalized polydispersity. From the best fit of experimental data, the modes of the micellar size distribution by volume were determined to be 2.8 nm at pH 6 and 2.2 nm at pH 8. The normalized polydispersities were 0.316 at pH 6 and 0.282 at pH 8. The median (and mean) values for the micellar size distribution by volume were calculated to be: 3.1 nm (and 3.3 nm) at pH 6 and 2.4 nm (and 2.5 nm) at pH 8. To check about the effect of temperature, we measured the micellar size distribution by DLS at 20 and 25 °C at pH 6. The obtained results are shown in Figure S5. It can be seen that small variations in temperature do not affect the volume size distribition at pH 6.

To determine the micellar size, we also used SAXS measurements, see Fig. 2**C**. The modeling of the obtained SAXS spectra was performed with SasView software using the following approach: (1) The measured scattering intensity, I, for scattering vector, q values between 0.02 and 0.05 $Å^{-1}$ was plotted as ln$I$ vs. ln$q$. The slope of the linear dependence of ln$I$ vs ln$q$ was determined. This slope is indicative of the shape of the formed aggregates [16]. When the slope is close to 0, a model for spherical micelles is used. If the slope is slightly positive, electrostatic interactions are included by using the Hayter_MSA correction. If the slope is −1, either an ellipsoidal model or a spherical model accounting for micellar aggregation via sticky hard sphere corrections is applied. (2) To determine the size and polydispersity of the micelles from the SAXS spectra, the scattering length densities (SLD) were fixed at 13.4 × 10^{-6} $Å^{-2}$ [2] for escin and 9.47 × 10^{-6} $Å^{-2}$ for water. (3) To start the fitting, initial values for the micellar radius and polydispersity were set to the values measured by DLS. The volume fraction was fixed at 0.05 for 5 wt % escin solutions and at 0.1 for 10 wt% escin solutions. (4) The fitting was performed with four free parameters: size, polydispersity, scale, and either charge (when accounting for electrostatic interactions) or stickiness (for aggregated spheres).

For SAXS spectra obtained from 5 wt% escin solutions at pH 6 and 8 the determined slopes of ln$I$ vs. ln$q$ were + 0.06 and + 0.3, respectively, showing the presence of individual objects of small size interacting via electrostatic repulsions. Therefore, the scattering curves were fitted with

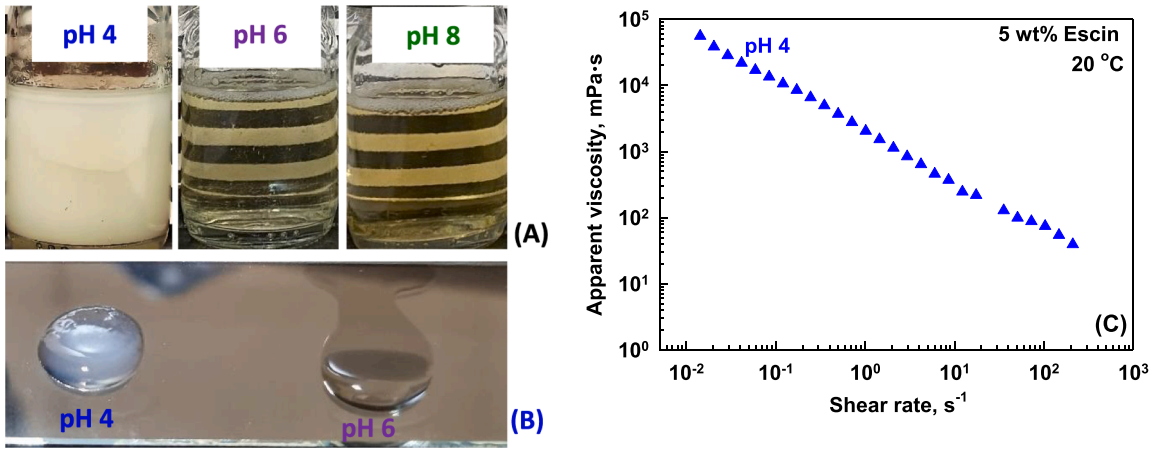

Fig. 1. (A) Illustrative pictures of prepared samples at three pHs. (B) A drop of samples prepared at pH 4 and pH 8 placed on the tilted microscopic glass (C) Apparent viscosity as a function of shear rate for 5 wt% escin solutions at pH 4.

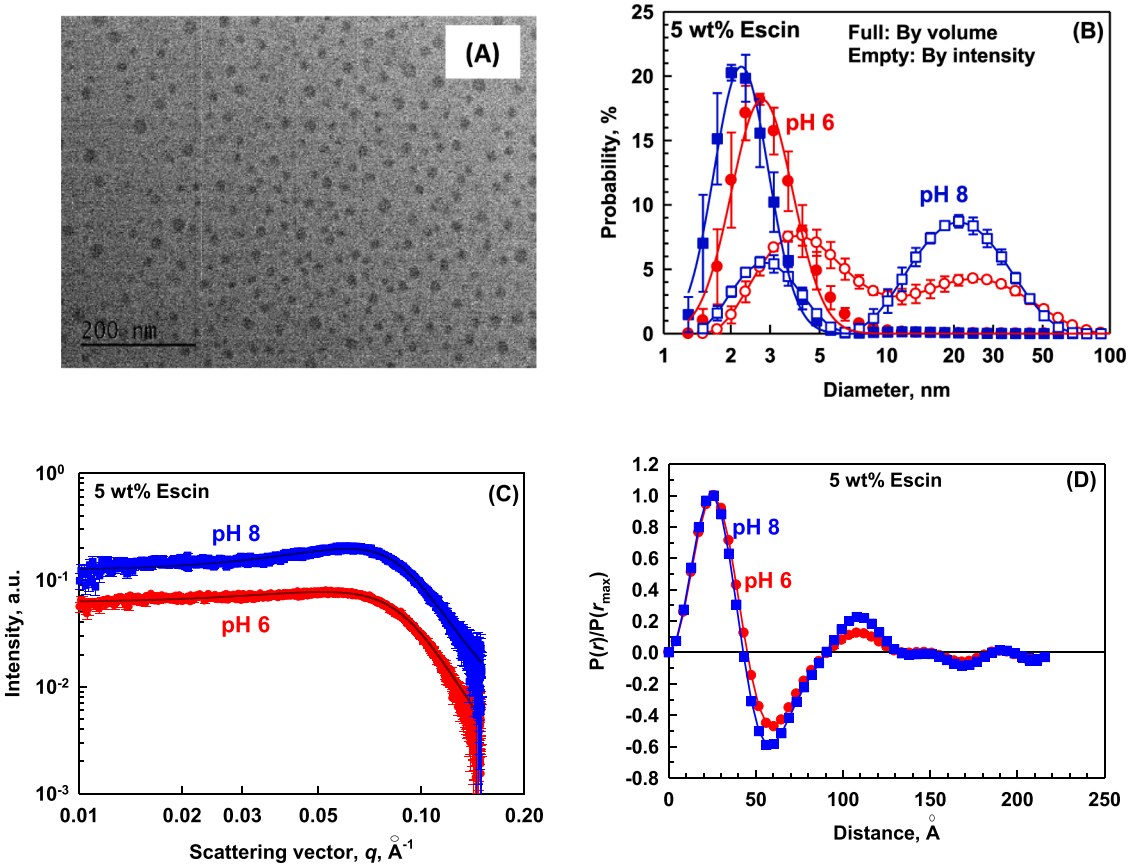

Fig. 2. (A) Cryo-TEM image of 5 wt% escin solution at pH 6; (B) Size distribution by volume (full symbols) and by intensity (empty symbols) as measured by DLS of 5 wt% escin solution at pH 6 (red circles) and pH 8 (blue squares). The lines for distribution by volume are the best fit of data by Eq. (1); (C) SAXS spectra measured for 5 wt% escin solution at pH 6 (red symbols) and at pH 8 (blue symbols) and best fits (continuous black curves) determined by SasView software with parameters shown in Table S1 in the SI; (D) Pair-distance distribution functions derived via Inverse Fourier transform with SasView software.

the sphere model implemented in SASView software with Hayter_MSA correction. From the best fits of the experimentally measured SAXS spectra, the median size of the micelles was determined to be 3.4 nm for pH 6 and 3.5 nm for pH 8. The scaled polydispersity was determined to be 0.40 for pH 6 and 0.36 for pH 8. These values are in good agreement with the results obtained from DLS measurements. The greater discrepancy in the median micellar size determined by DLS and SAXS at pH 8 (2.4 nm vs 3.5 nm) is most probably related to significant electrostatic repulsions between charged micelles which are known to significantly affect the sizes determined from DLS measurements [17]. It should be mentioned that although scattering intensity in SAXS is also proportional to the sixth power of the size, the model used to fit SAXS spectra gives a volume distribution. For this reason, micellar size distribution determined from the SAXS spectra fit does not detect the small fraction of 20 nm aggregates observed in cryo-TEM and in the DLS distribution by intensity. However, the presence of these aggregates is

seen in pair-distance distribution functions obtained from SAXS spectra, see Fig. 2**D**. The pair-distance distribution function is very sensitive to the maximum dimension of the aggregates. Consequently, a small fraction of 20 nm aggregates is seen in Fig. 2D, consistent with the results from the DLS intensity distribution and cryo-TEM images.

The number of charges per micelle is found to be 9.7 at pH 6 and 10.5 at pH 8. In order to determine the aggregation number of primary micelles we used the radius of micelles determined by SAXS measurements of 1.75 nm. The molecular volume of an escin molecule is assumed to be 1.878×10^{-27} m^3 (mass density of 1 g/ml is used for this estimation). This estimate shows that ≈ 12 molecules are incorporated in one primary micelle with size of 1.75 nm. Therefore, the determined charges for one aggregate at two different pH values show that more than 80 % of molecules are ionized at pH 6 and more than 88 % at pH 8. This high ionization of the molecules leads to formation of relatively small in size aggregate with a median diameter of 3.5 nm. To check the validity of the presence of charged micelles in escin solutions we measured the electrophoretic mobility of 5 wt% escin solutions at pH 6 and 8. The estimated ζ-potentials are -29 ± 3 mV at pH 8 and -26 ± 3 mV at pH 6, which supports the explanation that charged micelles form at pH > pKa.

To check about the effect of the polyphenols on the micellar size distribution, we performed experiments with an extract purchased from Sigma-Aldrich that does not contain polyphenols. The obtained experimental results are shown in Figure S5 and Table S1 in the SI. As can be seem, the distributions are similar, and the presence of 20–50 nm aggregates is observed in both samples.

Decreasing the pH below the pKa of escin molecules leads to the formation of turbid solutions with non-Newtonian behavior, as shown in Fig. 1**C**. Optical observations of solutions at pH 4 reveal a network of aggregates (Fig. 3**A**).

DLS measurements were performed on 10-fold diluted solutions, in which the formed network is disrupted. The resulting histograms by volume (Fig. 3**B**) show three well-defined peaks: one at approximately 80 nm, a second at 710 nm, and the largest at 5 μm. The largest peak at 5 μm is due to the breakage of the network, which leads to the formation of nearly spherical aggregates, as confirmed by optical observations of the diluted samples. The second peak at 710 nm is related to the thickness of the network observed in Fig. 3**A**. Cryo-TEM images (Fig. 3**C**) do not show the presence of 80 nm aggregates. This suggests that the sizes measured by DLS are due to the aggregation of smaller micelles.

SAXS spectra (Fig. 3**D**) shows that the curve for pH 4 does not level off at low scattering vectors, indicating that elongated objects are formed at low pH. The slope of ln$I$ vs ln$q$ for q values between 0.02 and 0.05 $Å^{-1}$ was determined to be −1. This slope shows formation of elongated micelles or/and aggregated micelles. When using the ellipsoidal model to fit the experimental data (Fig. 3**D**), the equatorial radius was determined to be 2.1 nm, while the polar radius was 5.5 nm, giving an aspect ratio of approximately 2.7. The SAXS spectra can also be well-fitted with a sticky hard sphere model. In that case, the radius of the primary micelles is 3.1 nm, with a stickiness of 0.15 and a log-normal scaled polydispersity of 0.199.

The formation of elongated micelles of nanometer size cannot explain the turbidity of the escin solutions at pH 4 nor the micrometer aggregates observed under the microscope. This experimental fact can be explained only by the formation of large aggregates. The neutralization of the carboxylic groups of the escin molecules at pH 4 removes

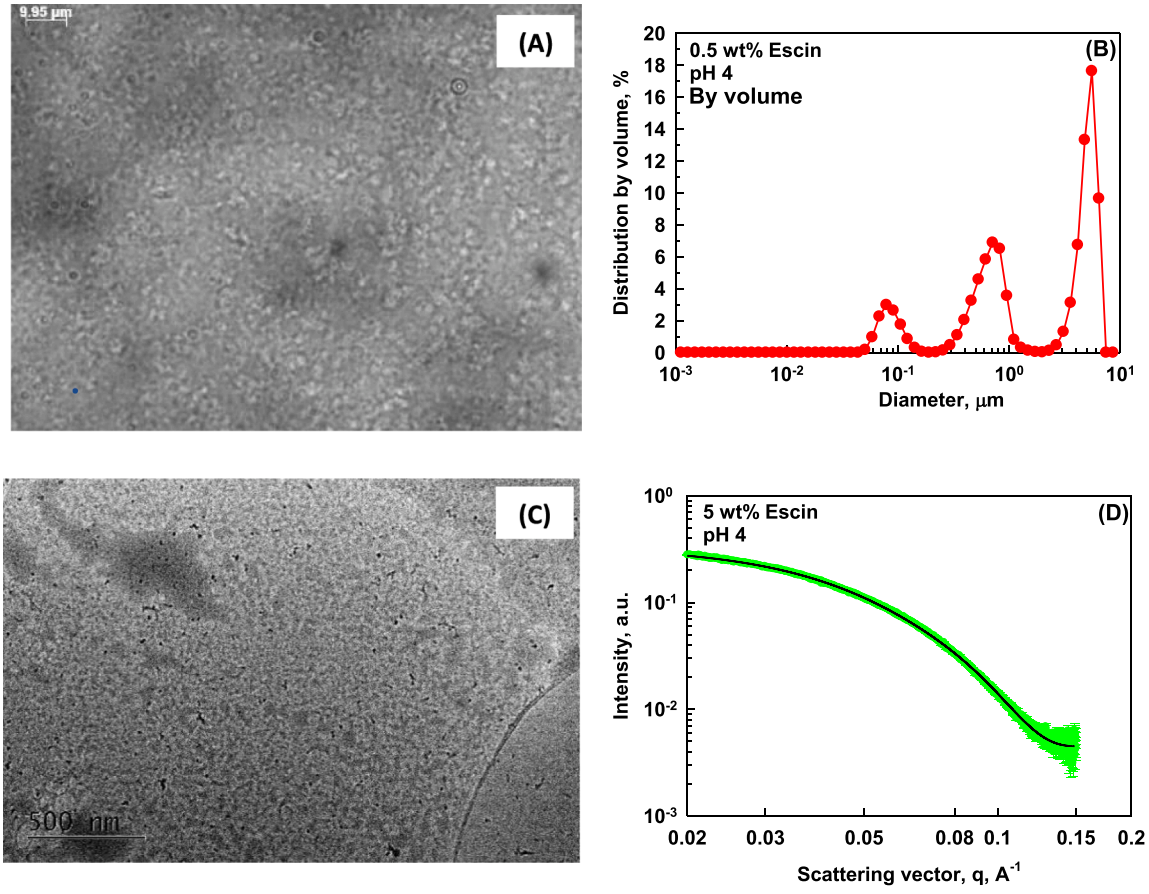

Fig. 3. (A) Illustrative picture of sample observed in transmitted light in thin layer formed from 5 wt% escin at pH 4. (B) Distribution by volume of 0.5 wt% escin solution at pH 4 prepared after 10-fold dilution with pure water; (C) Cryo-TEM image of solution containing 5 wt% escin at pH 4; (D) SAXS spectrum measured at 3000 mm sample to detector distance of 5 wt% escin solution at pH 4 (green symbols) and best fits (continuous black curve) determined by SasView software with parameters shown in Table S1 in the SI.

the charges from the micelle surfaces and decreases the repulsion between the micelles. This enables the formation of hydrogen bonds between escin molecules incorporated in two different micelles and ensures the adhesion of these micelles. As shown in Fig. 3 A and 3 C, these adhesive micelles form a network within the solution, which significantly increases its viscosity.

From these experiments we can conclude that escin solutions at pH 4 contains micrometer size aggregates that form a network in the solution, whereas at pHs of 6 and 8 the charge of carboxylic acid in escin molecule leads to negative charge on the surface of the micelles and prevents the formation of big in size aggregates and solutions remain transparent and stable for more than a month.

3.2. *Effect of KCl on properties of escin solutions at pH 6*

We studied the effect of potassium chloride (KCl) concentrations ranging from 100 to 1000 mM on 5 wt% (45 mM) escin solutions at pH 6. The addition of KCl significantly changed the visual appearance of the solutions, making them more turbid as the KCl concentration increased, see Figure S6 in the SI. Observations in transmitted light revealed the formation of a network-like structure within the solutions containing KCl. The size of the objects forming this network varied with concentration: the smallest objects were observed at 100 mM KCl, while well-defined entities, several micrometers in size, were visible in solutions with 500 and 1000 mM KCl, see Fig. 4. Cryo-TEM images of the 500 mM KCl solution confirmed the presence of aggregates of varying sizes and shapes, Fig. 4**D**, indicating significant aggregation when the electrolyte concentration is high enough to screen the electrostatic repulsions between the charged escin micelles.

SAXS spectra of solutions containing different KCl concentrations are shown in Fig. 5**A**. Normalized pair distribution functions shown in Fig. 5**B**, reveal the presence of small objects with core radius of ≈ 2.6 nm (no KCl), which increases to 3.0 nm in presence of 100 mM KCl and to 3.2 nm when 500 mM or 1000 mM KCl are added in the solution. Along with small changes in the core radius, the presence of bigger in size aggregates is well seen at high KCl concentrations, see Fig. 5**B**. The fit of experimentally determined SAXS spectra is also performed. For solution containing 100 mM KCl, we fit the spectrum assuming spherical objects with log-normal distribution which repeal each other in presence of 100 mM background electrolyte. This model describes very well the experimental data showing that the aggregation between primary micelles is very limited in this solution. The determined size is practically the same as one measured by DLS (4.8 vs. 4.4 nm) and the polydispersities are also very close (0.28 vs. 0.27), see Fig. 5. The spectra obtained in presence of 500 and 1000 mM KCl clearly show the presence of big aggregates in the samples as can be seen from the increased slope at low q values. The formation of big aggregates in solutions containing KCl is also well seen from DLS measurements performed with 10-fold diluted solutions for which the intensity weighted mean hydrodynamic diameter, Z_{ave}, increases from 4.6 nm (no KCl) to 100 nm in presence of 100 mM KCl and to 7500 nm for solutions containing 500 and 1000 mM KCl, Fig. 5**C.** The presence of micrometer size aggregates is also seen from the optical observations performed for diluted solutions (Figure S7 in the SI).

The rheological properties of prepared solutions with different KCl concentrations were also measured, see Figure S8 **in SI** and all prepared solutions showed shear thinning behavior as solutions prepared at pH 4. To determine the effect of KCl concentration on the apparent viscosity, we chose a shear rate of 100 s^{-1} . The shape of the viscosity vs. KCl concentration curve shown in Fig. 6 A remains consistent regardless of the shear rate chosen for determining apparent viscosity. The only significant difference is that at lower shear rates the values of apparent viscosity are higher. One sees that the viscosity passes through a maximum at 500 mM KCl, where the solutions remain turbid and stable over time and no phase separation is observed. The higher concentrations of KCl induce the phase separation as can be seen from pictures

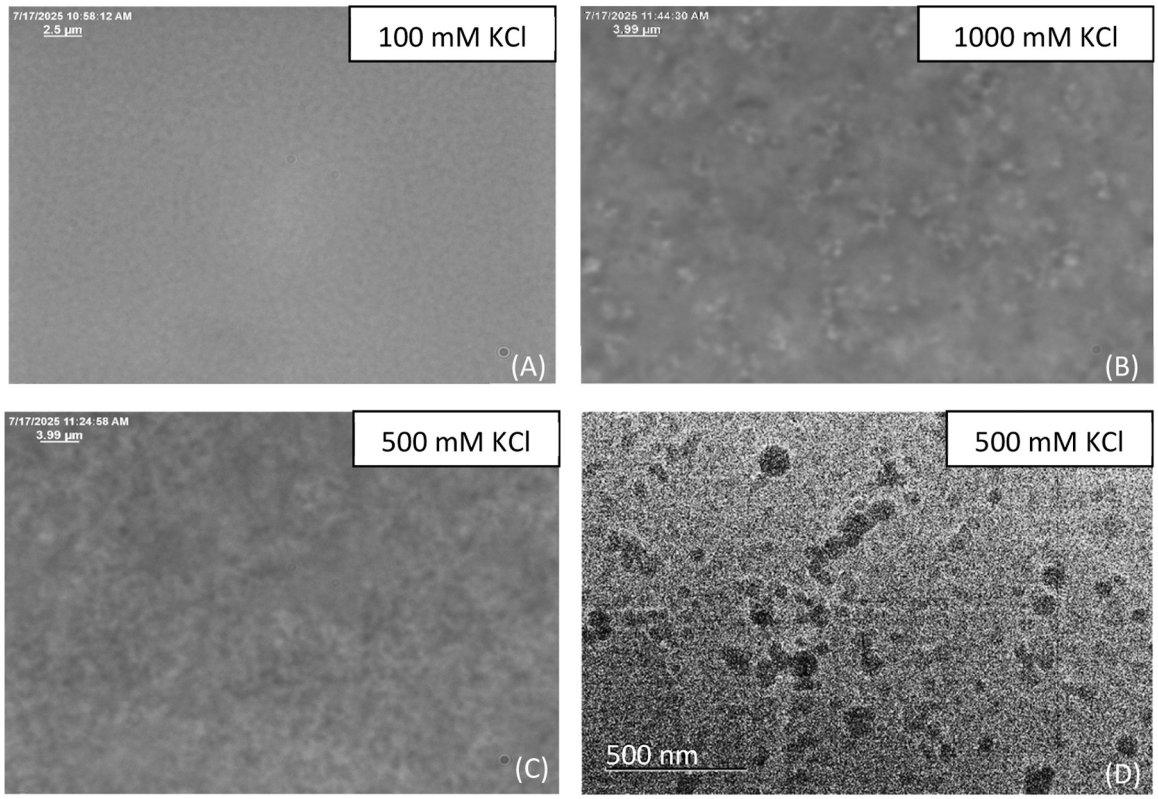

Fig. 4. Images from (A, B, C) observations in transmitted light of 5 wt% escin solutions at pH 6 after addition of (A) 100 mM KCl; (B) 1000 mM KCl and (C) 500 mM KCl. (D) Cryo-TEM image of solution containing 500 mM KCl.

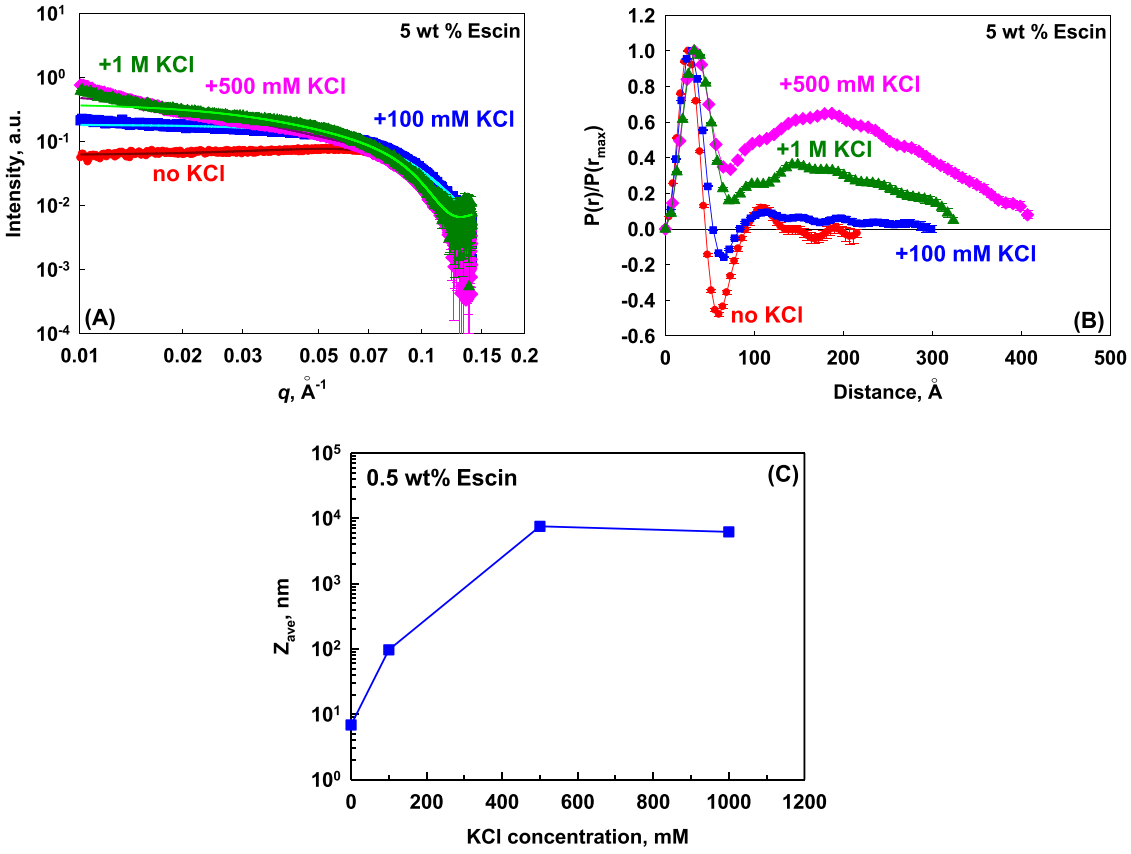

Fig. 5. (A) SAXS spectra and (B) Normalized pair distribution functions of 5 wt% escin solution without electrolyte (red symbols), in presence of 100 mM KCl (blue symbols), 500 mM KCl (pink symbols), and 1000 mM KCl (green symbols); (C) Intensity weighted mean hydrodynamic diameter, Z_{ave} measured by DLS for 10-times diluted solutions as a function of electrolyte concentration.

shown in Figure S9 in the SI. This behavior differs significantly from behavior of ionic surfactants in presence of electrolyte which form transparent solutions with cylindrical, branched or worm-like micelles [11,12]. It means that mechanism of the observed transition for conventional surfactants and escin solutions is different because of the completely different chemical structures of the molecules: long straight hydrophobic tail in the structures of conventional surfactants facilitates the formation of cylindrical type of micelles at high ionic strength. Whereas, the triterpenoid rigid hydrophobic part of the escin molecules prefers the formation of almost spherical micelles that afterwards can interact via hydrogen bonds to form secondary and ternary aggregates. Note that the formation of secondary micelles is well known phenomena for bile salts [18–21] which also have rigid hydrophobic part as steroid skeleton and OH-groups in the hydrophilic part of the molecule.

The rheological response of solutions with KCl concentrations between 400 and 600 mM, which are near the maximum in the salt curve shown in Fig. 6**A**, was investigated using frequency sweep (Fig. 6**B)** and amplitude sweep (Fig. 6**C)** experiments. The experimental results show that the tested solutions exhibit elastic behavior with the storage modulus, G', consistently higher than the loss modulus, G'', across the entire range of oscillation frequencies (between 0.02 and 4 Hz). This rheological response clearly shows that the increased viscosity of escin solutions at 400 and 500 mM KCl is not related to the formation of cylindrical, branched or worm-like micelles in these solutions. For solutions containing cylindrical, branched or worm-like micelles the viscous modulus, G'' is higher than G' at low frequency of oscillations and for worm-like micelles G'' passes through a maximum as a function of frequency of oscillation [22–25] which is not the case for escin solutions. As can be seen from data presented in Fig. 6, escin solutions with added KCl show the elastic behavior with G' being higher than G'' in the entire frequency range. The calculated $\tan\delta = G''/G'$ is constant as a function of a frequency of oscillation, which is typical for gel-like systems [26]. The values of tanδ decreases from 0.5 to 0.33 upon increasing KCl concentration from 400 to 500 mM for 5 wt% escin solutions, which shows the formation of space-spanning network around the maximum of the salt curve.

The rheological response of the escin solutions as a function of strain amplitude is displayed in Fig. 6**C**. At low strains, both moduli are independent of the shear strain and $G' > G''$ which is typical for gelled systems. Above a certain strain, G' begins to decrease, while G'' passes through a distinct maximum. This is the typical behavior observed in an attractive glass of electrostatically heteroaggregated systems [28–29].

To determine the yield stress of the samples, we used the crossover point at which $G' = G''$ and $\tan\delta = 1$, measured in amplitude sweep experiments (data shown in Fig. 6 C). Above this point the sample starts to flow. The obtained data are summarized in Table 1. The prepared solutions with KCl concentrations of 450 mM and 500 mM exhibit a yield stress of ≈ 2.4 Pa, whereas the yield stress decreases to 1.6 Pa upon the addition of 600 mM KCl. This decrease in yield stress is attributed to the strong interactions between the aggregates, leading to their separation over time.

Experimental data for stored solutions reveal different stability profiles depending on the KCl concentration relative to the maximum in the salt curve. Solutions with KCl concentrations before this maximum, remain stable upon storage. In contrast, solutions with concentrations after the maximum, exhibit phase separation after storage. Despite the phase separation, the apparent viscosity measured after storage and re-homogenization of the separated liquid layer shows no significant difference between samples stored for 1 day and 1 month (Fig. 6**A**). This indicates that the re-arrangement of the aggregates upon storage is

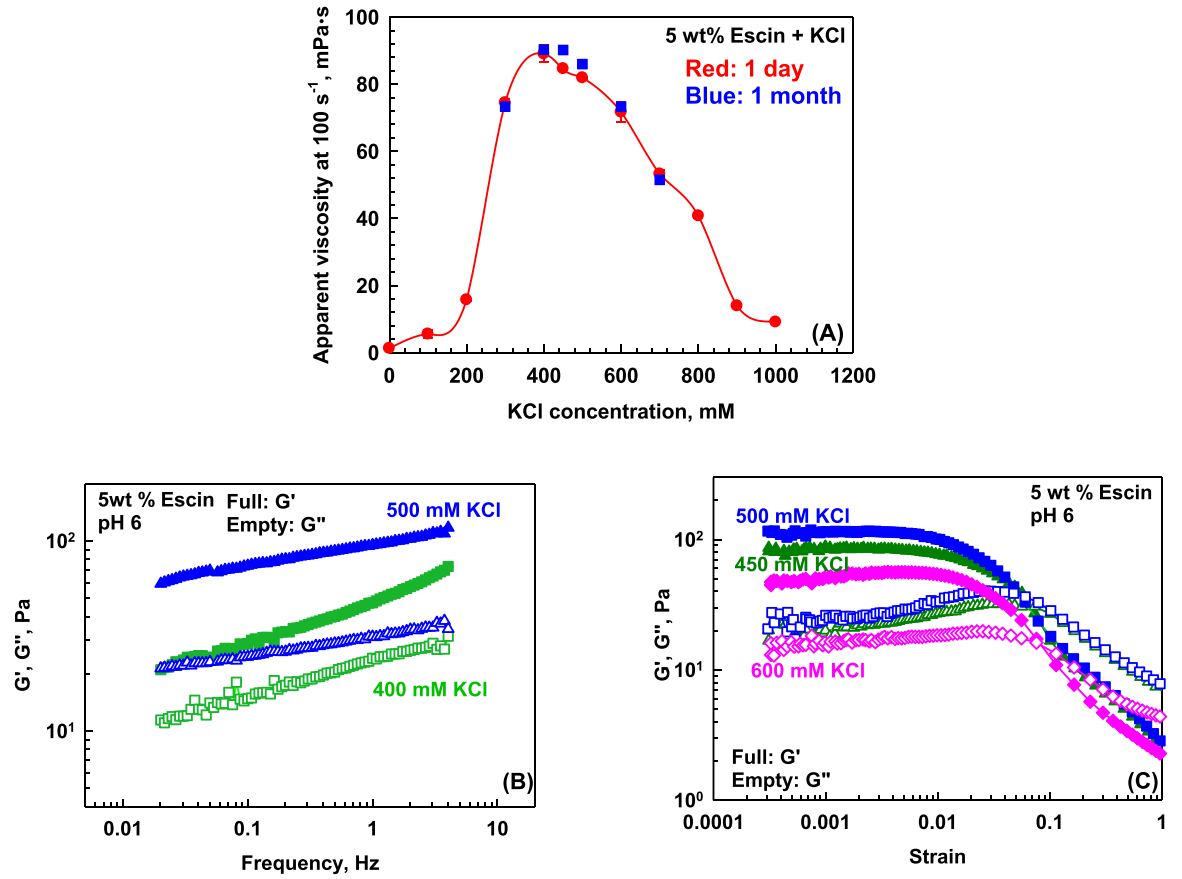

Fig. 6. (A) Apparent viscosity at 100 s^{-1} as a function of KCl concentration for 5 wt% escin solutions. (B) Storage and loss moduli as a function of frequency of oscillation at 1 % strain amplitude and (C) Storage and loss moduli as a function of strain amplitude at 1 Hz frequency of oscillation of 5 wt% escin solutions in presence of different KCl concentrations.

Table 1
Viscosity at 100 s^{-1}, yield stress, τ_0, elastic moduli at 0.1 % deformation, G' (0.1 % deformation), critical moduli, G_{CR} at the critical strain, γ_{CR} at which elastic and loss modulus become equal in amplitude sweep experiments for escin solutions at pH 6 in presence of 450, 500, and 600 mM KCl.

Parameter	KCl, mM			
	450	500	500	600
	5 wt% ESC	5 wt% ESC	10 wt% ESC	5 wt% ESC
Viscosity (100 s^{-1}), mPa•s	84.6 ± 0.3	81.9 ± 0.3	197.4 ± 32.2	71.7 ± 2.9
τ_0 (OSC), Pa	2.25 ± 0.13	2.39 ± 0.33	5.61	1.61 ± 0.26
G' (0.1 %), Pa	65 ± 20	97 ± 17	257	54 ± 3
G_{CR}, Pa	21 ± 8	32 ± 6	95	21 ± 4
γ_{CR}	0.065	0.054	0.083	0.076

reversible, and the apparent viscosity at high shear rates remains constant after re-homogenization. However, the apparent viscosity measured at low shear rates decrease significantly for samples containing KCl after the maximum. This is likely due to the re-homogenization step destroying the delicate structures that formed upon storage and are responsible for the resistance to flow at low shear stress.

From this series of experiments, we conclude that the addition of KCl to escin solutions decreases the electrostatic repulsion between the charged micelles. This decrease induces the formation of a space-spanning network throughout the entire volume when the KCl concentration is ≈ 500 mM. This network formation results in gelled samples that remain stable during prolonged storage. A further increase in electrolyte concentration leads to stronger aggregation, causing the network to begin collapsing, and the properties of the formed gels change over time.

3.3. *Effect of type of the electrolyte at pH 6*

It is well known from the literature that the peak position in dependence of the viscosity on salt concentration (salt curves) for conventional surfactants, depends on the valency and counterion radius [11,12, 30–32]. To check how the properties of escin micelles depends on the counterions, we performed the experiments with two mono- (Na^+ and K^+) and two divalent (Mg^{2+} and Ca^{2+}) counterions. Solutions with monovalent ions remained clear at an ionic strength of 100 mM, while those with divalent ions appeared opalescent. Increasing the ionic strength to 300 mM caused solutions with monovalent ions to become opalescent, while those with divalent ions became turbid. All solutions were homogeneous after overnight storage, with one exception: a solution with Ca^{2+} at an ionic strength of 300 mM formed crystals of calcium citrate. This crystallization occurred because the citric acid concentration (3.62 ± 0.42 g/l) in the solution exceeded the solubility of calcium citrate (0.96 g/l at 25 °C [33]). Due to this issue, we did not prepare solutions with higher Ca^{2+} concentrations for measurement.

All turbid solutions exhibited non-Newtonian behavior. The measured viscosity at a shear rate of 100 s^{-1} as a function of ionic strength for each electrolyte is presented in Fig. 7. For all systems, the viscosity passed through a maximum as the salt concentration increased, but the height and position of this peak were dependent on the specific electrolyte used. A more viscous solution was obtained in the presence of monovalent ions (K^+ or Na^+) than in the presence of the divalent ion

(Mg^{2+}). This effect has also been observed in mixtures of SLES+CAPB (sodium lauryl ether sulfate and cocamidopropyl betaine), where the carboxylic group of CAPB significantly impacts the conditions for micelle branching [12]. The much lower viscosity peak observed for escin solutions in presence of Mg^{2+} is attributed to its higher charge density, which facilitates the formation of an unstable network. When K^+ or Na^+ are used, they neutralize the carboxylic groups of the escin molecules and facilitate the formation of inter-micellar H-bonds which leads to formation of space-spanning network throughout the entire volume of the solution and this network remain stable up to 500 mM of monovalent ions. Similar situation is observed when the ionic strength is increased up to 300 mM by $MgCl_2$. However, the further addition of Mg^{2+} ions in the solution leads to formation of unstable network, because this counterion can neutralize two escin molecules from two different micelles and, along with H-bonds, can form Mg^{2+} bridges between them, which enhances the formation of the unstable network in the latter case.

From this series of experiments, we conclude that the apparent viscosity of escin solutions at pH > pKa exhibits a maximum as a function of electrolyte concentration. The higher viscosity is achieved when monovalent ions (K^+ or Na^+) are used to screen the electrostatic repulsions between the charged micelles. The lower viscosity observed in the presence of Mg^{2+} is explained by the possibility of forming inter-micellar Mg^{2+} bridges, which leads to the compaction of the aggregates and the eventual formation of an unstable network.

3.4. Effect of salt concentration at pH 4 and pH 8

Experiments were conducted to determine the effect of salt concentration on the rheological response of escin solutions at pH 4 and pH 8. The results show a significant difference in the viscosity-salt concentration curve shape at pH 4 compared to those at pH 6 and pH 8. At pH 4, the apparent viscosity is highest for solutions without added KCl, which is 73 mPa•s. Viscosity then decreases upon the addition of 100 mM KCl down to 60.4 mPa•s, and subsequently remains nearly constant at approximately 45 mPa•s for higher KCl concentrations. This distinct behavior is attributed to the fact that only around 16 % of the escin molecules are charged at pH 4. This low charge percentage significantly reduces the amount of KCl required to screen the electrostatic repulsions between escin micelles. The viscosity plateau observed at KCl concentrations above 200 mM is likely related to the presence of citric acid, used to adjust the pH. Ability of citric acid to form hydrogen bonds may prevent the formation of inter-micellar H-bonds, resulting in aggregates that cannot pack as efficiently as at higher pH and high ionic strength at pHs of 6 and 8.

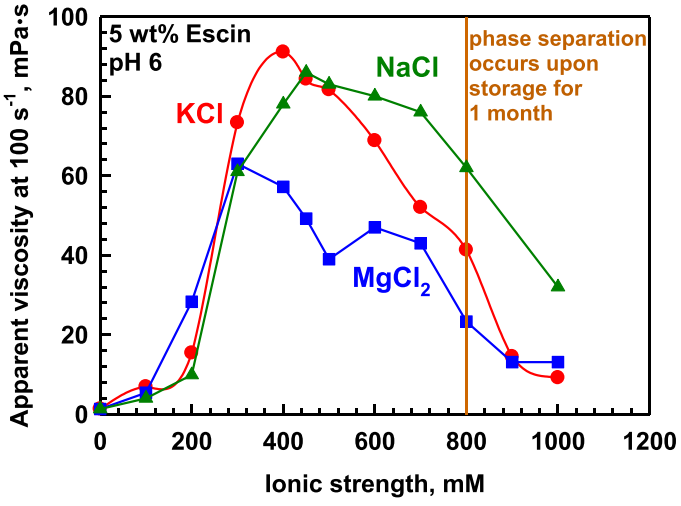

Fig. 7. Apparent viscosity at 100 s^{-1} as a function of ionic strength for the solutions with 5 wt% ESC at pH 6 in presence of NaCl (green triangles), KCl (red circles), and $MgCl_2$ (blue squares). Parallel to the *Y* axis orange line denotes the ionic strength at which phase separation upon storage is observed.

The peak in the viscosity-salt curve at pH 8 occurs at higher salt concentrations than at pH 6. This is due to the higher percentage of charged molecules at pH 8, which requires a higher electrolyte concentration to effectively screen the electrostatic repulsion between the charged micelles. The maximum viscosity achieved at pH 8 is also higher than at pH 6 due to a more difficult rearrangement of the micelles when the electrostatic repulsion is screened by the adsorption of counterions, compared to the case where a portion of the carboxylic groups is non-ionized.

From this series of experiments, we can conclude that the maximal viscosity at pH 4 is reached without added background electrolyte. This is due to the smaller fraction of ionized escin molecules at this pH. The increase in pH increases the fraction of ionized escin molecules, which consequently increases the electrolyte concentration needed to screen the electrostatic repulsions between the charged micelles. As a result, the maximal viscosity is reached only upon the addition of significant amount of background electrolyte at pH 6 and 8 (450 mM NaCl at pH 6 and 500 mM at pH 8) to the solutions.

3.5. Effect of escin concentration at pHs of 6 and 8

The rheological curves were measured for 10 wt% escin solutions at pH 8 containing varying NaCl concentrations. The prepared solutions exhibit non-Newtonian behavior. The apparent viscosity as a function of salt concentration is presented in Fig. 9**A**, along with results obtained for 5 wt% escin at pH 8. A two-fold increase in escin concentration leads to a more than 5.5 times increase in the maximal viscosity, which is reached in the presence of 450 mM NaCl. This substantial increase demonstrates the formation of a denser network at the higher escin concentration. The position of the viscosity maximum is not significantly affected by the escin concentration. This observation strongly indicates that the enhanced viscosity in escin solutions is not related to the formation of worm-like micelles. For worm-like micelles, an increase in surfactant concentration typically requires a lower electrolyte concentration to reach the maximal viscosity [23]. The fact that the viscosity maximum for escin solutions remains independent of the escin concentration suggests that the salt concentration is primarily required for screening the electrostatic repulsions between escin micelles. These micelles subsequently form aggregates via H-bonds. This contrasts with conventional surfactants, where the peak position shifts to lower salt concentrations at higher surfactant concentrations due to a change in the packing parameter of the molecules within the micelles.

The dependencies of the shear moduli *G'* and *G"* on the strain amplitude for escin solutions prepared at pH 6 in the presence of 500 mM KCl are shown in Fig. 9**B** for two escin concentrations of 5 wt% and 10 wt%. The increase in escin concentration results in higher values of both *G'* and *G"*, but the shape of the curves remains unchanged. This indicates that a denser space-spanning network is formed at the higher escin concentration. Furthermore, the yield stress determined for the 10 wt% escin solution is twice as high as that measured at 5 wt% escin concentration (see Table 1). The relatively weak dependence of all rheological characteristics shown in Table 1 on the increase in escin concentration suggests that the formed gels are positioned between weakly and strongly attractive systems. According to the analysis described in the literature [27], the storage modulus *G'* for strongly attractive emulsions increases with the oil volume fraction to the power of 1.5. This exponent is close to the value determined for the escin solutions when assuming that the two-fold increase in escin concentration leads to a two-fold increase in the fraction of big aggregates forming the space-spanning network.

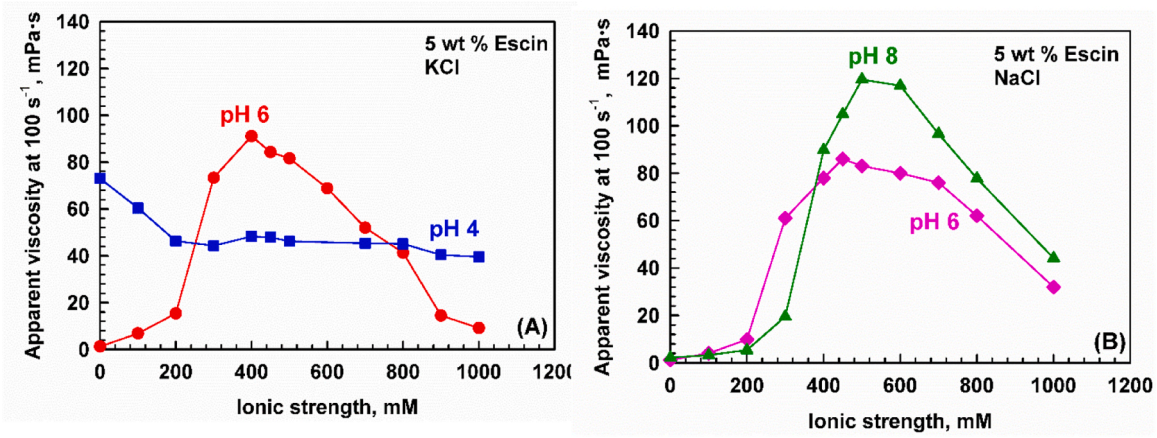

Fig. 8. Apparent viscosity at 100 s^{-1} as a function of ionic strength for the solutions with 5 wt% ESC at (A) pH 4 (blue squares) and pH 6 (red circles) in presence of KCl and (B) pH 6 (pink diamonds) and pH 8 (green triangles) in presence of NaCl.

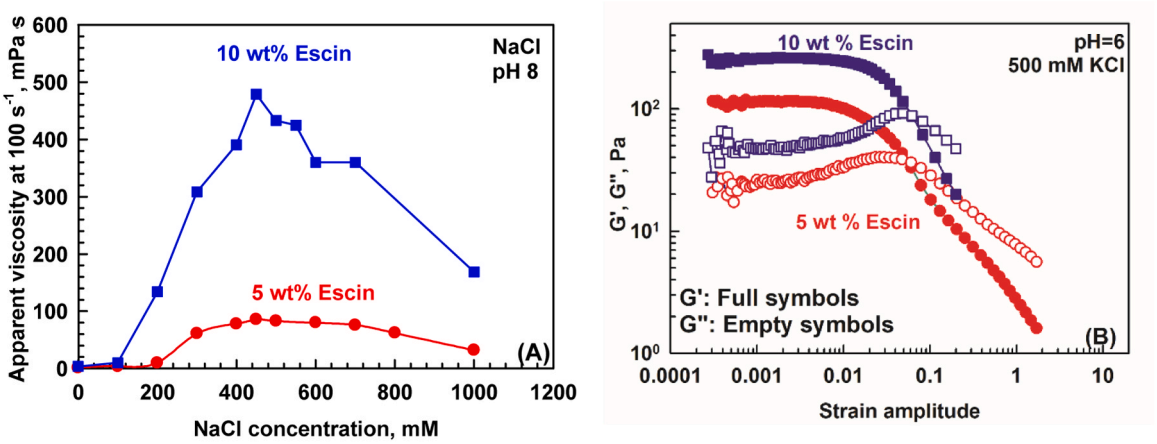

Fig. 9. (A) Apparent viscosity at 100 s^{-1} of shear rate as a function of salt concentration at pH 8 with 5 wt% (red circles) and 10 wt% (blue squares) of escin. (B) Shear elastic (G′) and shear loss (G″) moduli as a function of strain amplitude for escin solutions at 5 wt% (red circles) and 10 wt% (blue squares) escin solutions in presence of 500 mM KCl at pH 6. All measurements are performed at 20 °C.

4. Discussions

The difference between saponins and conventional anionic surfactants is related to their different chemical structure: the conventional surfactants have long hydrophobic hydrocarbon chain while the escin has triterpenoid hydrophobic skeleton and voluminous hydrophilic residues. Escin molecules are more similar to the bile salts structures which are steroids with non-conjugated or conjugated hydrophilic parts with different amino acids [18]. Those bio-surfactants are known to form so-called primary micelles (diameter < 2 nm) which upon further increase in the concentration are assembled in secondary micelles [18]. Their shape is confirmed by molecular dynamic simulations [21, 34–35].

Escin shows behavior as nonionic and anionic surfactant depending on the solution pH. This difference in the micelles formed from ionized and non-ionized escin molecules is related to the differences in the forces acting between charged and uncharged micelles. When the molecules are non-ionized, the primary micelles are uncharged and escin molecules from two micelles can form inter-micellar H-bonds which leads to formation of aggregates in the solutions and non-Newtonian behaviour. However, when the molecules are ionized, the charged micelles are formed and electrostatic repulsions between them do not allow formation of inter-micellar H-bonds and as consequence intra-molecular and intra-micellar H-bonding is preferable.

The effect of electrolyte is also different for the two types of molecules: ionized or non-ionized. The addition of salt to charged escin micelles leads to viscosity increase. Thus, salt curves could be measured for ionized escin molecules. However, the reason for viscosity increase is different from that of the conventional surfactants where screening of the electrostatic interactions changes molecules packing parameter which results in worm-like micelles formation [11,12,24–26,30–32]. For conventional surfactants the addition of counterion decreases the area per molecule within the micelles but this does not result in formation of H-bonding between the molecules incorporated in two different micelles. For escin molecules the addition of counterion decreases the electrostatic repulsion between charged micelles which enables the formation of H-bonds between the escin molecules incorporated in two different micelles and leads to formation of bigger aggregates. Observations by optical and cryo-transmission electron microscopes, revealed that network of large agglomerates was formed by the attracted primary micelles which is schematically illustrated in Fig. 10. Note that the main difference with the conventional surfactants is that the latter transform from spherical to worm-like micelles. On the other hand, the initial spherical escin micelles arrange into large aggregates as a span network upon electrolyte addition. The worm-like micelles solutions are clear and isotropic at all ionic strengths and do not phase separate overtime [11,12, 24–26,30–32], whereas the formation of big aggregates with size above 500 nm in escin solutions leads to formation of turbid solutions which starts to phase separate when the concentration of background electrolyte becomes so high that the

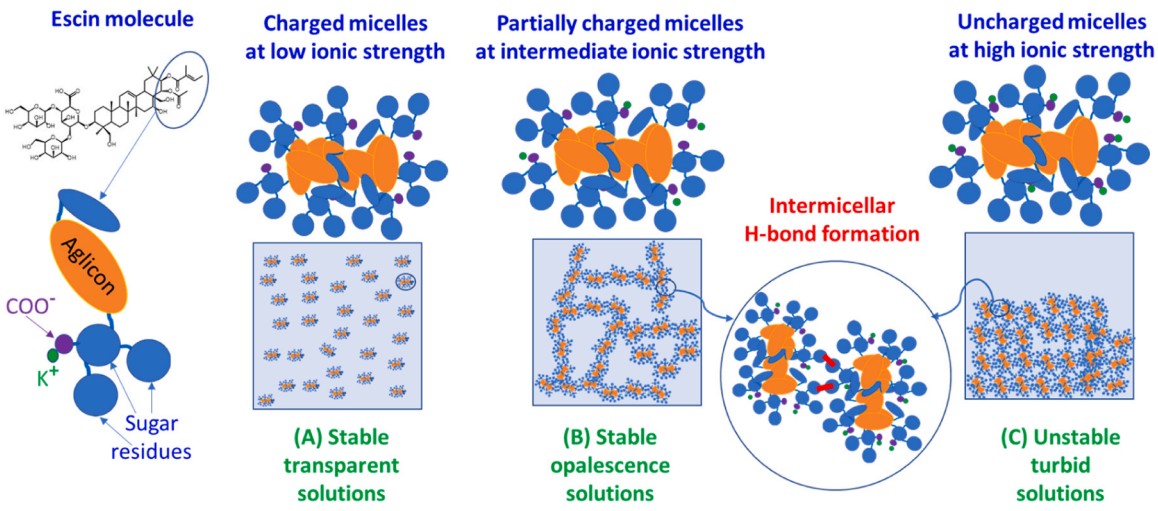

Fig. 10. Schematic representation of the transformation of the micelles in the solution of ionized escin upon addition of electrolyte in cases of (A) no electrolyte or low electrolyte concentrations, low-viscous Newtonian solution containing spherical micelles, (B) maximum viscosity at the peak of the salt curve where micellar network is formed, and (C) at the highest electrolyte concentration, dropped-down viscosity because of phase separation of the aggregates due to formation of intermicellar H-bonds.

aggregates can rearrange and compact due to formation of bigger in number inter-micellar H-bonds.

5. Conclusions

Solutions containing ionized (pH > pKa) and non-ionized (pH < pKa) escin molecules were studied. It was found that non-ionized escin molecules at pH 4 form nanometer sized micelles which aggregate and form turbid, viscous solutions that exhibit non-Newtonian behavior with maximal viscosity reached when there is no background electrolyte added in the solution. In contrast, deprotonation of the single carboxylic group in the molecule increases escin solubility, leading to the formation of small spherical micelles (~ 4 nm) in clear, water-like solutions with Newtonian behavior at pH of 6 and 8.

The addition of background electrolyte has relatively small effect on the properties of the escin solution at pH 4 due to lower fraction of ionized molecules at this pH. The apparent viscosity measured at 100 s^{-1} for 5 wt% escin solutions decreases from 73 mPa•s to 45 mPa•s upon increase of KCl from 0 to 200 mM and it remains constant afterwards causing phase separation of prepared solutions upon storage at ambient temperature.

The addition of background electrolyte to solutions of ionized escin molecules at pH 6 and 8 switches the rheological behavior from Newtonian to non-Newtonian. Similar to the conventional anionic surfactants, the viscosity of the escin solutions at pH > pKa passes through a maximum with increasing electrolyte concentration.

However, the solutions of conventional surfactants remain clear upon salt addition due to formation of worm-like micelles, whereas the escin solutions become turbid due to formation of micrometer aggregates. Escin dispersions at the viscosity maximum remain stable for at least one month at ambient temperature, whereas those with higher electrolyte concentrations above the maximum phase separate upon storage.

To the best of our knowledge, this alternative mechanism of viscosity increase in a non-conventional surfactant is reported here for the first time. Considering the advantages of escin as a biodegradable plant extract with unique surface and biological activities, the systems explored in this study hold promise as templates for diverse detergent and cosmetic formulations.

CRediT authorship contribution statement

Slavka Tcholakova: Writing – review & editing, Supervision, Project administration, Methodology, Funding acquisition, Formal analysis, Conceptualization. **Petar Borisov:** Visualization, Validation, Methodology, Investigation, Formal analysis. **Zlatina Mitrinova:** Writing – review & editing, Visualization, Validation, Methodology, Investigation. **Fatmegul Mustan:** Writing – original draft, Visualization, Validation, Methodology, Investigation, Formal analysis.

Funding

This study was partially funded by the European Union-NextGenerationEU, through the National Recovery and Resilience Plan of the Republic of Bulgaria, project No BG-RRP-2.004–0008.

Declaration of Competing Interest

The authors declare that they have no known competing financial interests or personal relationships that could have appeared to influence the work reported in this paper.

Acknowledgments

The support of the Centre of Competence “Sustainable Utilization of Bio-resources and Waste of Medicinal and Aromatic Plants for Innovative Bioactive Products” (BIORESOURCES BG), project BG16RFPR002–1.014–0001, funded by the Program “Research, Innovation and Digitization for Smart Transformation” 2021–2027, co-funded by the EU, is greatly acknowledged.

ZM acknowledges project BG16RFPR002–1.014–0006 "National Centre of Excellence Mechatronics and Clean Technologies", co-funded by the European Union, under Program "Research Innovation and Digitization for Smart Transformation" program 2021–2027. The authors are grateful to Mrs. Kristina Rusanova and Assoc. Prof. Lyuben Mihaylov (Sofia University) for cryo-TEM imaging.

Appendix A. Supporting information

Supplementary data associated with this article can be found in the online version at doi:10.1016/j.colsurfa.2026.139730.

Data availability

Data will be made available on request.

References

[1] K. Hostettmann, A. Marston, SAPONINS in Encyclopedia of Analytical Science (Second Edition), Elsevier, 2005, pp. 205–209, https://doi.org/10.1016/B0-12-369397-7/00548-3.

[2] C. Dargel, R. Geisler, Y. Hannappel, I. Kemker, N. Sewald, T. Hellweg, Self-assembly of the bio-surfactant aescin in solution: A small-angle X-ray scattering and Fluorescence study, Colloids Interfaces 3 (2019) 47, https://doi.org/10.3390/colloids3020047.

[3] K. Golemanov, S. Tcholakova, N. Denkov, E. Pelan, S.D. Stoyanov, Remarkably high surface visco-elasticity of adsorption layers of triterpenoid saponins, Soft Matter 9 (2013) 5738–5752, https://doi.org/10.1039/c3sm27950b.

[4] N. Pagureva, S. Tcholakova, K. Golemanov, N. Denkov, E. Pelan, S.D. Stoyanov, Surface properties of adsorption layers formed from triterpenoid and steroid saponins, Colloids Surf. A 491 (2016) 18–28, https://doi.org/10.1016/j.colsurfa.2015.12.001.

[5] S. Tcholakova, F. Mustan, N. Pagureva, K. Golemanov, N.D. Denkov, E.G. Pelan, S. D. Stoyanov, Role of surface properties for the kinetics of bubble Ostwald ripening in saponin-stabilized foams, Colloids Surf. A 534 (2017) 16–25, https://doi.org/10.1016/j.colsurfa.2017.04.055.

[6] S. Tsibranska, A. Ivanova, S. Tcholakova, N. Denkov, Structure of dense adsorption layers of escin at the air-water interface studied by molecular dynamics simulations, Langmuir 35 (2019) 12876–12887, https://doi.org/10.1021/acs.langmuir.9b02260.

[7] D. Glikman, N. García Rey, M. Richert, K. Meister, B. Braunschweig, pH effects on the molecular structure and charging state of β-Escin biosurfactants at the air-water interface, J. Colloid Interface Sci. 607 (2022) 1754–1761, https://doi.org/10.1016/j.jcis.2021.09.086.

[8] R. Geisler, C. Dargel, T. Hellweg, The Biosurfactant β-Aescin: A Review on the Physico-Chemical Properties and Its Interaction with Lipid Model Membranes and Langmuir Monolayers, Molecules 25 (2020) 117, https://doi.org/10.3390/molecules25010117.

[9] C. de Groot, M. Müsken, C.C. Müller-Goymann, Novel Colloidal Microstructures of β-Escin and the Liposomal Components Cholesterol and DPPC, Planta Med 84 (2018) 1219–1227, https://doi.org/10.1055/a-0624-2706.

[10] I.M. Tucker, A. Burley, R.E. Petkova, S.L. Hosking, J.R.P. Webster, et al., Self-assembly in escin-nonionic surfactant mixtures: From micelles to vesicles, J. Colloid Interface Sci. 626 (2022) 305–313, https://doi.org/10.1016/j.jcis.2022.06.122.

[11] M. Pleines, W. Kunz, T. Zemb, D. Benczedi, W. Fieber, Molecular factors governing the viscosity peak of giant micelles in the presence of salt and fragrances, J. Colloid Interface Sci. 537 (2019) 682–693, https://doi.org/10.1016/j.jcis.2018.11.072.

[12] Z. Mitrinova, H. Alexandrov, N. Denkov, S. Tcholakova, Effect of counter-ion on rheological properties of mixed surfactant solutions, Colloids Surf. A Physicochem. Eng. Asp. 643 (2022) 128746, https://doi.org/10.1016/j.colsurfa.2022.128746.

[13] M. Kondo, H. Minamino, G. Okuyama, K. Honda, H. Nagasawa, Y. Otani, Physicochemical properties and applications of and I-glycyrrhizins, natural surface active agents in licorice root extract, J. Soc. Cosmet. Chem. 37 (1986) 177–189.

[14] K. Matsuoka, R. Miyajima, Y. Ishida, S. Karasawa, T. Yoshimura, Aggregate formation of glycyrrhizic acid, Colloids Surf. A 500 (2016) 112–117, https://doi.org/10.1016/j.colsurfa.2016.04.032.

[15] I.M. Tucker, A. Burley, R.E. Petkova, S.L. Hosking, J. Penfold, et al., Adsorption and self-assembly properties of the plant based biosurfactant, Glycyrrhizic acid, J. Colloid Interface Sci. 598 (2021) 444–454, https://doi.org/10.1016/j.jcis.2021.03.101.

[16] Y. Fan, Y. Wang, Applications of small-angle X-ray scattering/smallangle neutron scattering and cryogenic transmission electron microscopy to understand self-assembly of surfactants, Curr. Opin. Colloid Interface Sci. 42 (2019) 1–16, https://doi.org/10.1016/j.cocis.2019.02.011.

[17] K.S. Birdi (Ed.), Handbook of Surface and Colloid Chemistry, 4th ed., CRC Press, 2015 https://doi.org/10.1201/b18633.

[18] D.M. Small, Size and Structure of Bile Salt Micelles, Adv. Chem. 84 (1968) 31–52, https://doi.org/10.1021/ba-1968-0084.ch004.

[19] M.C. Carey, D.M. Small, Micelle Formation by Bile Salts. Physical-chemical and Thermodynamic Considerations, Arch. Intern. Med. 130 (1972) 506–527.

[20] D. Madenci, S. Egelhaaf, Self-assembly in aqueous bile salt solutions, Curr. Opin. Colloid Interface Sci. 15 (2010) 109–115, https://doi.org/10.1016/j.cocis.2009.11.010.

[21] F. Mustan, A. Ivanova, S. Tcholakova, Taurodeoxycholate aggregation explored by molecular dynamics: Primary-to-secondary micelle transition and formation of mixed micelles with fatty acids, Molecules 29 (2024) 5897, https://doi.org/10.3390/molecules29245897.

[22] M.E. Cates, S.J. Candau, Statics and dynamics of worm-like surfactant micelles, J. Phys. Condens. Matter 2 (1990) 6869, https://doi.org/10.1088/0953-8984/2/33/001.

[23] L.M. Walker, Rheology and structure of worm-like micelles, Curr. Opin. Colloid Interface Sci. 6 (5-6) (2001) 451–456, https://doi.org/10.1016/S1359-0294(01)00116-9.

[24] K.D. Danov, G.M. Radulova, J.T. Petkov, Y.W. Ung, On the rheology of linear wormlike micellar solutions, JCIS Open (2025) 100160, https://doi.org/10.1016/j.jciso.2025.100160.

[25] T.N. Stancheva, M.T. Georgiev, G.M. Radulova, K.D. Danov, K.G. Marinova, Rheology of saturated micellar networks: Wormlike micellar solutions vs. bicontinuous micellar phases, Colloids Surf. A 652 (2022) 129927, https://doi.org/10.1016/j.colsurfa.2022.129927.

[26] H.H. Winter, M. Mours, Rheology of Polymers Near Liquid-Solid Transitions, in: Neutron Spin Echo Spectroscopy Viscoelasticity Rheology. Advances in Polymer Science, 134, Springer, Berlin, Heidelberg, 1997, https://doi.org/10.1007/3-540-68449-2_3.

[27] P.L. Fuhrmann, S. Breunig, G. Sala, L. Sagis, M. Stieger, et al., Rheological behaviour of attractive emulsions differing in droplet-droplet interaction strength, J. Colloid Interface Sci. 607 (2022) 389–400, https://doi.org/10.1016/j.jcis.2021.08.124.

[28] C. Christopoulou, G. Petekidis, B. Erwin, M. Cloitre, D. Vlassopoulos, Ageing and yield behaviour in model soft colloidal glasses, Philos. Trans. R. Soc. A 367 (2009) 5051–5071, https://doi.org/10.1098/rsta.2009.0166.

[29] K. Hyun, S.H. Kim, K.H. Ahn, S.J. Lee, Large amplitude oscillatory shear as a way to classify the complex fluids, J. NonNewton. Fluid Mech. 107 (2002) 51–65, https://doi.org/10.1016/S0377-0257(02)00141-6.

[30] E. Warmbier-Wytykowska, et al., How Do the Valency and Radii of Cations Affect the Rheological Properties of Aqueous Solutions of Zwitterionic and Anionic Surfactant Mixtures? Langmuir 41 (2025) 3561–3571.

[31] X. Tang, W. Zou, P.H. Koenig, S.D. McConaughy, M.R. Weaver, D.M. Eike, M. Schmidt, R.G. Larson, Multiscale modeling of the effects of salt and perfume raw materials on the rheological properties of commercial threadlike micellar solutions, J. Phys. Chem. B 121 (11) (2017) 2468–2485.

[32] L. Abezgauz, K. Kuperkar, P.A. Hassan, O. Ramon, P. Bahadur, D. Danino, Effect of Hofmeister anions on micellization and micellar growth of the surfactant cetylpyridinium chloride, J. Colloid Interface Sci. 342 (2010) 83–92.

[33] R.C. Weast (Ed.), Handbook of Chemistry and Physics, 57th ed., CRC Press Inc, Cleveland, 1976, p. B-99.

[34] D. Warren, D.K. Chalmers, K. Hutchison, W. Dang, C.W. Pouton, Molecular Dynamics Simulations of Spontaneous Bile Salt Aggregation, Colloids Surf. A 280 (2006) 182–193, https://doi.org/10.1016/j.colsurfa.2006.02.009.

[35] L. Partay, M. Sega, P. Jedlovszky, Morphology of Bile Salt Micelles as Studied by Computer Simulation Methods, Langmuir 23 (2007) 12322–12328, https://doi.org/10.1021/la701749u.